

Diagnosing temporal quantum correlations: compressed non-Markovian calipers

G. A. L. White,^{1,*} F. A. Pollock,² L. C. L. Hollenberg,¹ C. D. Hill,^{1,3,†} and K. Modi^{2,‡}

¹*School of Physics, University of Melbourne, Parkville, VIC 3010, Australia*

²*School of Physics and Astronomy, Monash University, Clayton, VIC 3800, Australia*

³*School of Mathematics and Statistics, University of Melbourne, Parkville, VIC, 3010, Australia*

The complete characterisation of non-Markovian dynamics on quantum devices can be achieved with experiments on the system using a procedure known as process tensor tomography. However, through either hardware or computational restrictions, tomographically complete estimation is usually out of reach. Here, we present methods for bounding any desired facet of multi-time processes only with limited data to arbitrary accuracy that depends on data availability. We then use this method to estimate the strength of non-Markovian memory and construct conditional Markov order models, which are far less complex yet possess high predictive power. Finally, we display the efficacy and utility of our theoretical methods with experimental case studies on IBM Quantum devices.

Introduction.— Achieving error rates requisite for fault-tolerant error correcting codes is a significant milestone goal in the scale-up of quantum devices. One of the major hurdles to this effect is the taming of correlated – either spatially or temporally – noise in quantum hardware [1–3]. The former has a robust theoretical basis, but the latter, often called non-Markovian noise, is only recently beginning to emerge as a more serious consideration [4–7]. In this Letter, we present an array of tools to probe different aspects of non-Markovianity, each with a clear interpretation, on quantum devices. These results are based on process tensor tomography (PTT), which is possible through a procedure we introduce in our adjoining Article [8] for characterisation of multitime quantum stochastic processes. We implement these diagnostics as part of a broader theoretical result to cover hardware and scaling drawbacks of PTT. In the spirit of compressed sensing, we evaluate processes consistent with some limited set of data. Importantly, this case of tomographically incomplete data not only reduces experimental burden, it is crucial for most current hardware that lack fast measure-and-feed-forward protocols. Further, estimating robust non-Markovian measures scales exponentially poorly in the number of time steps. As an alternative, we introduce a family of efficient measures based on the concept of quantum Markov order [9]. These approaches each come equipped with exact bounds of desired tightness for any facet of temporal correlations.

Specifically, we first develop a method to explore the space of full processes who are consistent with some limited data. As a consequence, we are able to find minimum and maximum bounds on meaningful objective functions of the process in a way that resembles a caliper. These bounds may be arbitrarily tight – depending both on the purity of the process and the accessible span of observations – and are useful for determining the strength and character of the non-Markovian noise. Next, we examine the question of ‘how much does a limited memory model fail to predict observations seen in the laboratory?’. This fine-grains previous results which typically answer the yes/no question of Markovianity with some

confidence [10, 11]. Instead, we quantify the number of previous process steps which must be accounted for in order to describe the dynamics up to some desired approximation. Importantly, these measures have both simple interpretations, and a clear recipe to expand the model should they fail to adequately explain the data.

While our theoretical frameworks are hardware-agnostic, we implement these methods on the IBM Quantum Experience. Our findings indicate these devices to be non-Markovian, with effects made more complex by the introduction of crosstalk, and correlations which increasingly build up over time. Remarkably, this noise is not only correlated, it is naturally bipartite entangled in time, a signature of genuinely quantum non-Markovianity.

Process tensor tomography.— In any given experiment, there is a distinction between the controllable operations implemented by the experimenter on a d -dimensional system, and the uncontrollable stochastic dynamics due to system-environment (SE) interactions. A quantum stochastic process accounts for quantum correlations across a number of times $\mathbf{T}_k := \{t_0, \dots, t_k\}$. Such processes are represented as a multilinear map from a sequences of controllable operations on a system of dimension d to a final state density matrix. Here, the map, known as a process tensor [12, 13], represents all of the uncontrollable dynamics of the process. Through a generalisation of the Choi-Jamiolkowski isomorphism (CJI) [14], this mapping is encapsulated by its Choi state $\Upsilon_{k:0}$ over k time steps as a correlated multipartite density operator. Its two-time marginals are completely positive, trace-preserving (CPTP) maps $\hat{\mathcal{E}}_{j+1:j}$ for each sequential pair in \mathbf{T}_k , as well as average initial state ρ_0 . Each marginal has an input and an output tensor leg, starting from the initial state. Collectively, we label these $\{\mathbf{o}_k, \mathbf{i}_k, \mathbf{o}_{k-1}, \dots, \mathbf{i}_1, \mathbf{o}_0\}$ and depict the state in Figure 1a.

The operations that drive an experiment can be represented generically by a set of CP maps $\{\mathcal{A}_0, \mathcal{A}_1, \dots, \mathcal{A}_{k-1}\}$ such that the Choi state of the full sequence is given by $\mathbf{A}_{k-1:0} = \bigotimes_{i=0}^{k-1} \mathcal{A}_i$. The final output, conditioned on these operations, is then given by the

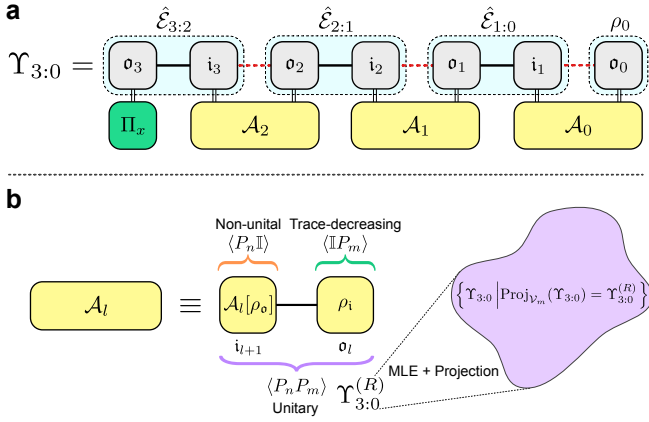


FIG. 1. **a** The generalised Choi state of a 3-step process tensor. This object represents a sequence of possibly correlated CPTP maps between different points in time, as well as average initial state. Each output leg o_l is mapped by a control operation \mathcal{A}_l to the next input leg i_{l+1} . **b** Partitioning the Choi states of operations into non-unital, trace-decreasing, and unitary operations illustrates what observables of $\Upsilon_{3:0}$ are obtained from different controls. Unitary-only characterisation generates a family of process tensors consistent with the data, found through MLE.

spatiotemporal generalisation of Born’s rule [15]:

$$\rho_k(\mathbf{A}_{k-1:0}) = \text{Tr}_{\text{in}} [\Upsilon_{k:0} (\mathbb{I}_{\text{out}} \otimes \mathbf{A}_{k-1:0}^{\text{T}})]. \quad (1)$$

This generalises joint probability distributions of a classical stochastic process to the quantum regime [16]. Importantly, the description does not average over any SE dynamics or initial correlations, meaning that it naturally describes any arbitrarily strong non-Markovian dynamics.

On quantum devices, this object may be reconstructed using PTT, formalised in our accompanying Article [8]. Since it is a linear operator, it is fully determined by its input-output relations on an informationally complete (IC) basis of sequences of CP maps. In this, the Choi representation is constructed and temporal correlations are directly mapped onto spatial ones, allowing for standard spatial quantum information tools to be applied to the space of temporal processes, giving rise to formal measures of non-Markovianity [17] and other properties of the process, which we detail in Table I and discuss in Results sections.

Optimising over the consistent space.— When Equation (1) is measured experimentally for a quorum, $\mathcal{O}(d^{4k})$, of control sequences, the process tensor is uniquely fixed and one can then straightforwardly quantify the non-Markovian correlations [18]. Most experiments, however, can only implement an undercomplete control basis; this might be a forced constraint – for example, unitary operations tend to be the only high quality operations available on NISQ devices. Or, one might like to reduce the experimental overhead with the increas-

ing inclusion of data until bounds on chosen objectives are sufficiently tight.

Our aim is to infer a full process and quantify non-Markovian correlation therein from given limited data. The space of k -step process tensors is given through the CJI by the set of $2k+1$ -partite density matrices satisfying causality conditions. Specifically, they are unit-trace positive matrices satisfying

$$\text{Tr}_{o_j} [\Upsilon_{j:0}] = \mathbb{I}_{i_j} \otimes \Upsilon_{j-1:0} \quad \forall j \in \{1 : k\}. \quad (2)$$

Physically, these causality conditions ensure that averaging over future operations does not affect the statistics of the past. Mathematically, they generate a hyperplane of dimension $\sum_{j=1}^k (d^2 - 1)d^{4j-2}$ (the number of zero values in the Pauli basis) plus one for normalisation [8]. Let this affine space be denoted by \mathcal{V}_c .

In an accompanying Article [8], we developed a projection routine as part of maximum likelihood estimation (MLE) to impose $\Upsilon_{k:0} \in \mathcal{S}_n^+ \cap \mathcal{V}_c$. The main theoretical result of this Letter is to extend this in two ways here: first, we expand the affine space to include observed data, and second, we consider a range of different information-theoretic quantities as our objective to find maxima and minima. This opens up exploration of the family of process tensors consistent with the limited observations. The technique functions generically, however for concreteness we consider the restriction of unitary-only control sequences followed by a terminating measurement, as in Figure 1.

Consider a process tensor with decomposition

$$\Upsilon_{k:0} = \Upsilon_{k:0}^{(R)} + \Upsilon_{k:0}^{(R_{\perp})}, \quad (3)$$

where $\Upsilon_{k:0}^{(R)}$ is fixed by a restricted set of experimental observations, and $\Upsilon_{k:0}^{(R_{\perp})}$ its free (modulo physical constraints) orthogonal complement. In the CJI picture, unitary operations preserve the entanglement of the Bell state. Thus, there are $d^4 - 2d^2 + 2$ nontrivial Pauli terms – the weight-2 operators and $\langle \mathbb{I} \rangle$. Equation (1) shows how the action of a process tensor constitutes projecting its Choi state onto the Choi state of the sequence. Correspondingly, the operation \mathcal{A}_l gives expectation values relevant to indices i_{l+1} and o_l . Figure 1b illustrates the partitioning of operations with respect to nontrivial Pauli expectations: the set of non-unital maps $\langle P_n \mathbb{I} \rangle$, the stochastic or trace-decreasing maps $\langle \mathbb{I} P_m \rangle$, and the unitary maps $\langle P_n P_m \rangle$. This elucidates the relevance of different types of quantum operations to different aspects of the process, such as marginals and correlations terms.

Now, suppose we have probed a process solely without an IC basis. Then, after treating the data with MLE, we have a set of observations $p_i, \bar{\mu}$ corresponding to our restricted basis $\mathfrak{B} := \{\mathbf{B}_{k-1:0}^{\bar{\mu}}\} := \{\otimes_{j=0}^{k-1} \mathcal{B}_j^{\mu_j}\}$ and POVM $\mathcal{J} := \{\Pi_i\}$. We can construct a new affine space \mathcal{V}_m from

Setup	QMI (min, max)	Negativity	Purity	Fidelity	Conditional QMI*
#1. System Alone	(0.298, 0.304)	(0.0179, 0.0181)	(0.8900, 0.8904)	(0.9423, 0.9427)	(0.158, 0.178)
#2. $ +\rangle$ Nearest Neighbours (NN)	(0.363, 0.369)	(0.0255, 0.0259)	(0.7476, 0.7485)	(0.7239, 0.7244)	(0.161, 0.224)
#3. Periodic CNOTs on NNs in $ +\rangle$	(0.348, 0.358)	(0.0240, 0.0246)	(0.7796, 0.7811)	(0.7264, 0.7272)	(0.180, 0.211)
#4. $ 0\rangle$ NNs with QDD	(0.358, 0.373)	(0.0205, 0.0210)	(0.8592, 0.8612)	(0.8034, 0.8045)	(0.196, 0.221)
#5. $ +\rangle$ Long-range Neighbours	(0.329, 0.339)	(0.0209, 0.0214)	(0.8594, 0.8608)	(0.9252, 0.9260)	(0.173, 0.190)
#6. $ +\rangle$ NN, delay, $ +\rangle$ next-to-NN	(0.322, 0.329)	(0.0209, 0.0213)	(0.8534, 0.8549)	(0.9077, 0.9083)	(0.168, 0.185)

TABLE I. Bounds on properties of process tensor Choi states with different background dynamics. QMI measures the non-Markovianity of the process, meanwhile conditional QMI indicate the maximal and minimal decoupling of the first and third time steps of the MLE estimate for some unitary control operation \mathcal{A}_1 . Negativity is a measure of the unbound temporal bipartite entanglement. Purity of the Choi state gives purity of the ensemble of open system trajectories, while fidelity captures the level of noise. * Only the MLE estimate was used here, the minimum and maximum are over the space of operations, not process tensor families.

these observations, given by

$$\left\{ \Upsilon_{k:0} \in \mathbb{C}^{n \times n} \mid \text{Tr} \left[\Upsilon_{k:0} \left(\Pi_i \otimes \mathbf{B}_{k-1:0}^{\mu T} \right) \right] = p_{i,\mu} \right\} \quad (4)$$

$$\forall \Pi_i \in \mathcal{J}, \mathbf{B}_{k-1:0}^{\mu} \in \mathfrak{B}.$$

The generation of this is depicted in Figure 1b. Consequently, the family of process tensors which are consistent with our observations is given by the intersection of the cone \mathcal{S}_n^+ and the affine space $\mathcal{V} := \mathcal{V}_c \oplus \mathcal{V}_m$. As in our accompanying Article, this allows us to use a projection routine to optimise some chosen objective function over the feasible set using the `pgdb` algorithm [8, 19]. In short, we perform gradient descent with the function of interest, where at each iteration the object is projected onto $\mathcal{S}_n^+ \cap \mathcal{V}$. Akin to a caliper shifting across a region to measure, using this technique we find minimum and maximum bounds for the values that any differentiable function can take for all process tensors consistent with the observed data.

Demonstration. – To demonstrate this approach on experimental data, we constructed six three-step (four time) process tensors in different dynamical setups for a single system qubit on the superconducting device *ibmq-casablanca*. These setups were designed to examine the base non-Markovianity, as well as the influence of crosstalk in a variety of situations. The basis was restricted to ten unitaries per time step, for a total of 3000 circuits per process tensor at 4096 shots, and a process tensor estimated with MLE. Keeping these restricted observations fit, we then searched the family of consistent process tensors for a variety of diagnostic quantities.

Specifically, we consider five information-theoretic quantities: (i) To measure the total amount of non-Markovianity, we employ quantum relative entropy, $S(\rho \parallel \sigma) := \text{Tr} [\rho(\log \rho - \log \sigma)]$, between $\Upsilon_{k:0}$ and the product of its marginals $\bigotimes_{j=1}^k \hat{\mathcal{E}}_{j:j-1} \otimes \rho_0$. This is a generalisation of quantum mutual information (QMI) beyond the bipartite scenario and is endowed with a clear operational meaning [17]. (ii) To determine whether the non-Markovianity has genuine quantum features we quantify the entanglement in the process [20, 21] by means of neg-

ativity, $\max_{\Gamma_B} \frac{1}{2} (\|\Upsilon_{k:0}^{\Gamma_B}\|_1 - 1)$, where Γ_B is the partial transpose across some bipartition [22]. (iii) We compute the purity of the process, $\text{Tr} [\Upsilon_{k:0}^2]$, to measure both the strength and size of non-Markovianity through the purity of the ensemble of non-Markovian trajectories. (iv) Finally, to quantify both Markovian and non-Markovian noise over multiple time steps we compute the distance between the desired process and the noisy process, we compute the fidelity, $\text{Tr} [\Upsilon_{k:0} (\bigotimes_{j=1}^k |\Psi\rangle\langle\Psi| \otimes \rho_{\text{ideal}})]$ with $|\Psi\rangle = |00\rangle + |11\rangle$, which compares the fidelity of the process with respect to the ideal Choi state. Our results are summarised in Table I.

Surprisingly, we find these bounds to be extremely tight. This appears to be due to the relative purity of the process, with ranks (to numerical threshold of 10^{-8}) of between 44 and 68 for the 128×128 matrix MLE estimates. Sets for positive solutions to low rank underdetermined systems have been studied in Ref. [23], and famously in compressed sensing for quantum state tomography [24]. As well as tightening bounds, the rank of the process is directly related to the size of environment, with each nontrivial eigenvector constituting a dynamical trajectory. In practice, then, this can both compress requirements and estimate the effective dimension of the non-Markovian bath.

Interestingly, the QMI is much larger than zero in all situations. Moreover, we compute the negativity across the middle cut of the Choi state (between leg \mathbf{i}_2 and \mathbf{o}_1) and find this to be entangled in all cases. Thus, not only are these noisy stochastic processes non-Markovian, they are bipartite quantum entangled in time. This includes Experiment #1, where no action is taken on the surrounding qubits, suggesting that there is non-Markovian behaviour present even beyond the immediate effects of crosstalk. Crosstalk certainly increases correlation strength, as well as decreasing process fidelity – an effect shown by switching neighbours into the $|+\rangle$ state and coupling to ZZ noise. But ZZ noise alone cannot generate temporal entanglement [14]. We remark in particular that when a quadratic dynamical decoupling (QDD) protocol [25] is performed on neighbouring qubits

in Experiment #4 with X and Y gates, the QMI increases with respect to the other experiments, but fidelity is not as low as in #2 or #3. This may suggest that naive QDD reduces the strength but increases the complexity of the noise, warranting further studies.

Although we developed this procedure in principle to bound generic processes, in practice, we find near complete determination for only relatively few numbers of measurements. In general, an IC three-step process tensor requires 12 288 circuits, but with only unitary gates this is 3000, so the savings are substantial. For limited quantum computing resources, one might consider measuring more and more basis sequences until the bounds given for memory were satisfactorily tight. This supplements, for example, machine learning approaches to directly estimate the memory [26, 27] or full characterisations [18]. With the nearly unique estimate, in the final column of the table, we also compute the maximum and minimum instrument-specific memory in the form of conditional QMI (CQMI), i.e., the QMI of the Choi state when the second step is projected onto some variable unitary operation as in Figure 2a. CQMI bounds the strength of non-Markovian memory [28], which then quantifies our ability to decouple from the non-Markovian noise. Moreover, the minimal CQMI is largest for #4, suggesting that naively attempting to decouple these systems may sometimes produce a less controllable system, consistent with the observations of, e.g., Ref [29]. Nevertheless, we can leverage the size of CQMI to construct reduced memory (and complexity) models for processes.

Rigorous model violation.— The CQMI from Table I indicates that conditionally finite memory processes may suffice to describe dynamics on IBM Quantum devices. In classical stochastic processes, this is known as Markov order. If marginalising over all but the previous ℓ time-steps produces the same statistics for the current time as the full joint statistics, then the process is said to have Markov order ℓ . Here, this means only the previous ℓ operations are relevant to the current statistics.

Our approach for efficient non-Markovian estimation is to construct increasingly complex models, and quantify how well they describe the observed dynamics on the device. This measure is computationally convenient, scaling linearly in time-steps (exponential in memory length); has an immediately available interpretation; and may be performed up to an acceptable approximation, or where costs become prohibitive. In the quantum case, processes cannot generically exhibit Markov order. Instead, they may have a property known as *conditional* Markov order [9]. Consider three groupings of \mathbf{T}_k : the past P with marginal Υ_P , the memory M with marginal Υ_M , and the future F , Υ_F . When a quantum process has conditional Markov order ℓ , then for $|M| = \ell$, and

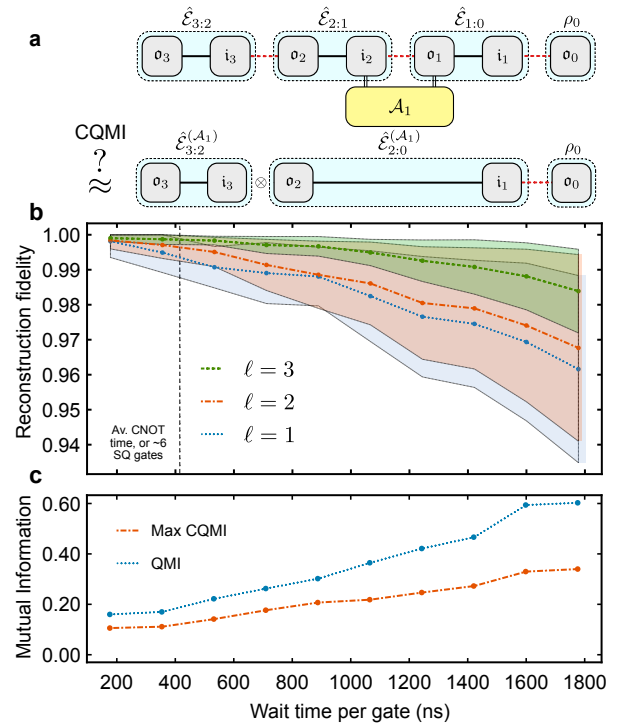


FIG. 2. Build-up of temporal correlations with increasing interaction time. **a** A depiction of the CQMI, which quantifies the error in truncating correlations beyond $\ell = 2$ when conditioned on intermediate operations. **b** A four step process is considered with increasing wait time after each gate. Using Markov orders $\ell = 1$, $\ell = 2$, and $\ell = 3$, we quantify how each model reconstructs the process across 100 random unitary sequences. Points indicate average fidelity, shaded regions indicate standard deviation. **c** QMI and CQMI both increase with interaction time, respectively bounding the breakdown of $\ell = 1$ and $\ell = 2$ models.

some sequence \mathbf{C}_M acting on the memory

$$\text{Tr}_M [\Upsilon_{FMP} \mathbf{C}_M^T] = \Upsilon_F^{(\mathbf{C}_M)} \otimes \Upsilon_P^{(\mathbf{C}_M)}, \quad (5)$$

where parentheses indicate a process conditional on the choice \mathbf{C}_M . This equality can only be exact for a single IC basis, but may be approximately true for arbitrarily many control operations. The magnitude of approximation is indicated by the CQMI. In this case, only Υ_{MP} and Υ_{FM} are necessary, which is a more efficient description of the process. In our accompanying Article we extend the theory of quantum Markov order further by deriving a method by which overlapping memory blocks may be stitched together, and a procedure for estimating these models [8]. A conditional Markov order ℓ model may be constructed by performing PTT on blocks $M_0 := \{t_0, \dots, t_\ell\}$, $M_1 := \{t_1, \dots, t_{\ell+1}\}$, \dots , $M_{k-\ell} := \{t_{k-\ell}, \dots, t_k\}$. The estimated process tensors then collectively account for all correlations in groups of ℓ sequential time steps in the object $\Upsilon_{k:0}^\ell := \{\Upsilon_{k:k-\ell}, \Upsilon_{k-1:k-\ell-1}, \dots, \Upsilon_{\ell+1:1}, \Upsilon_{\ell:0}\}$. Modelling a dynamical process in this manner allows one

to study the effects of omitting any longer time correlations [30].

We performed this procedure as an example on *ibmq-guadalupe* to observe the build-up of correlations as a function of time. For a four step (five time) process, we constructed process tensors $\Upsilon_{4:0}^\ell$ for $\ell \in \{1, 2, 3\}$. The neighbouring qubit to the system was initialised in a $|+\rangle$ state, and the duration of each step varied. We perform this for ten different times, ranging from 180 ns up to 1800 ns for a total of $2 \times 3000 \times 10 = 60000$ circuits for the $\ell = 3$ case. For each value of t , we executed 100 sequences of random unitaries $\{\mathbf{U}_{3:0}^i\}$ followed by state reconstruction. Then the action of $\Upsilon_{4:0}^\ell$ on $\mathbf{U}_{3:0}^i$ is used to predict the resulting state of each sequence. The fidelity between predicted state and actual state is computed, and the distribution for each data point is shown in Figure 2. We see here the behaviour that temporal correlations build up in a quantum stochastic process. The timescales seen here constitute relatively short-depth effective circuits, meaning these temporal correlations are likely to accumulate and spread out across practical circuits. Interestingly, the $\ell = 3$ model performs significantly better than the other two, whereas $\ell = 2$ is only marginally better at predicting the dynamics than $\ell = 1$ [31]. This suggests that most of the memory effects in these devices are higher order – they persist across multiple times. Because of the cumulative build-up, for long-time dynamical processes in real situations, mitigating the effects of these correlations would require either decoupling early, or fine-graining the process into many more time steps. The effects of these temporal correlations manifest themselves over a time frame of only a few CNOT gates, indicating that non-Markovian dynamics are likely a significant class of noise in regular circuits.

Markovianity breakdown has been previously quantified in terms of model violation in gate sets, or in the breakdown of CP divisibility [32–34]. However these approaches only coarsely diagnose temporal correlations, and are not generic to the process (i.e. they are only in terms of either specific gates, or no gates at all). We have presented a systematic framework by which different levels of finite conditional Markov order may be tested on quantum devices with both a rigorous foundation and a practical interpretation.

Conclusions. – In this work, we have introduced a host of techniques to diagnose and work with temporal correlations on near-term quantum processors. The flexibility of our approach is that the desired accuracy and computational requirements are at the experimenters discretion. A future approach might be to frame the question in terms of statistical quantities, allowing one to place confidence on the quality of different finite Markov models [35]. One might also find it useful to further inspect individual sequences who are better or worse predicted by the various models as an indication of the type of noise, and which operations sharpen these correlated effects.

Further, we have initiated an approach to compressed descriptions of the dynamics with confidence, but it would be more desirable to have a methodical approach to determining minimal required information for a multi-time process, up to some error.

Our results on IBM Quantum devices show that non-Markovian correlations steadily build as the circuit depth increased. This prompts the need for further study of temporally correlated errors and non-Markovian behaviour on NISQ devices. This diagnostic framework can both help facilitate this, and, as indicated in Ref. [8], mitigate the effects of open systems on these devices. Understanding and addressing this complex behaviour is a necessary step on the path to fault tolerance.

Acknowledgments. – This work was supported by the University of Melbourne through the establishment of an IBM Quantum Network Hub at the University. G.A.L.W. is supported by an Australian Government Research Training Program Scholarship. C.D.H. is supported through a Laby Foundation grant at The University of Melbourne. K.M. is supported through Australian Research Council Future Fellowship FT160100073. K.M. and C.D.H. acknowledge the support of Australian Research Council’s Discovery Project DP210100597. K.M. and C.D.H. were recipients of the International Quantum U Tech Accelerator award by the US Air Force Research Laboratory.

* white.g@unimelb.edu.au

† cdhill@unimelb.edu.au

‡ kavan.modi@monash.edu

- [1] N. H. Nickerson and B. J. Brown, *Quantum* **3**, 131 (2019), [arXiv:1712.00502](https://arxiv.org/abs/1712.00502).
- [2] K. Rudinger, T. Proctor, D. Langharst, M. Sarovar, K. Young, and R. Blume-Kohout, *Phys. Rev. X* **9**, 021045 (2019).
- [3] C. T. Chubb and S. T. Flammia, *Annales de l’Institut Henri Poincaré (D) Combinatorics, Physics and their Interactions* **8**, 269 (2021), [arXiv:1809.10704](https://arxiv.org/abs/1809.10704).
- [4] R. Harper, S. T. Flammia, and J. J. Wallman, *Nature Physics* **16**, 1184 (2020), [arXiv:1907.13022](https://arxiv.org/abs/1907.13022).
- [5] G. A. L. White, C. D. Hill, F. A. Pollock, L. C. L. Hollenberg, and K. Modi, *Nature Communications* **11**, 6301 (2020), [arXiv:2004.14018](https://arxiv.org/abs/2004.14018).
- [6] B. D. Clader, C. J. Trout, J. P. Barnes, K. Schultz, G. Quiroz, and P. Titum, *Physical Review A* **103**, 052428 (2021), [arXiv:2101.11631](https://arxiv.org/abs/2101.11631).
- [7] U. von Lüpke, F. Beaudoin, L. M. Norris, Y. Sung, R. Winik, J. Y. Qiu, M. Kjaergaard, D. Kim, J. Yoder, S. Gustavsson, L. Viola, and W. D. Oliver, *PRX Quantum* **1**, 010305 (2020).
- [8] G. A. L. White, F. A. Pollock, L. C. L. Hollenberg, K. Modi, and C. D. Hill, [arXiv:2106.11722v1](https://arxiv.org/abs/2106.11722v1).
- [9] P. Taranto, F. A. Pollock, S. Milz, M. Tomamichel, and K. Modi, *Physical Review Letters* **122**, 140401 (2019).
- [10] R. Blume-Kohout, K. Rudinger, E. Nielsen, T. Proctor, and K. Young, [arxiv:2012.12231](https://arxiv.org/abs/2012.12231) (2020).

- [11] E. Nielsen, J. K. Gamble, K. Rudinger, T. Scholten, K. Young, and R. Blume-Kohout, [arXiv:2009.07301 \(2020\)](#).
- [12] F. A. Pollock, C. Rodríguez-Rosario, T. Frauenheim, M. Paternostro, and K. Modi, [Physical Review A **97**, 012127 \(2018\)](#), [arXiv:1512.00589](#).
- [13] F. Costa and S. Shrapnel, [New Journal of Physics **18**, 063032 \(2016\)](#).
- [14] S. Milz and K. Modi, [PRX Quantum \(2021\)](#), [arXiv:2012.01894](#).
- [15] S. Shrapnel, F. Costa, and G. Milburn, [New Journal of Physics **20**, 053010 \(2018\)](#).
- [16] S. Milz, F. Sakuldee, F. A. Pollock, and K. Modi, [Quantum **4**, 255 \(2020\)](#), [arXiv:1712.02589](#).
- [17] F. A. Pollock, C. Rodríguez-Rosario, T. Frauenheim, M. Paternostro, and K. Modi, [Physical Review Letters **120**, 040405 \(2018\)](#), [arXiv:1801.09811](#).
- [18] L. Xiang, Z. Zong, Z. Zhan, Y. Fei, C. Run, Y. Wu, W. Jin, C. Xiao, Z. Jia, P. Duan, J. Wu, Y. Yin, and G. Guo, [arXiv:2105.03333 \(2021\)](#).
- [19] G. C. Knee, E. Bolduc, J. Leach, and E. M. Gauger, [Physical Review A **98**, 062336 \(2018\)](#), [arXiv:1803.10062](#).
- [20] C. Giarmatzi and F. Costa, [Quantum **5**, 440 \(2021\)](#).
- [21] S. Milz, C. Spee, Z.-P. Xu, F. A. Pollock, K. Modi, and O. Gühne, [SciPost Phys. **10**, 141 \(2021\)](#).
- [22] Entanglement across indices \mathfrak{o}_j , i_j will trivially be large for nearly unitary processes. We care about the entanglement across indices i_j , \mathfrak{o}_{j-1} , which measures coherent quantum memory effects between time steps.
- [23] M. Wang, W. Xu, and A. Tang, [IEEE Transactions on Signal Processing **59**, 1007 \(2011\)](#).
- [24] S. T. Flammia, D. Gross, Y.-K. Liu, and J. Eisert, [New Journal of Physics **14**, 095022 \(2012\)](#), [arXiv:1205.2300](#).
- [25] J. R. West, B. H. Fong, and D. A. Lidar, [Phys. Rev. Lett. **104**, 130501 \(2010\)](#).
- [26] C. Guo, K. Modi, and D. Poletti, [Physical Review A **102**, 062414 \(2020\)](#).
- [27] K. Goswami, C. Giarmatzi, C. Monterola, S. Shrapnel, J. Romero, and F. Costa, [arXiv preprint arXiv:2102.01327 \(2021\)](#).
- [28] P. Taranto, F. A. Pollock, and K. Modi, [\(2019\)](#), [arXiv:1907.12583](#).
- [29] P. Jurcevic, A. Javadi-Abhari, L. S. Bishop, I. Lauer, D. F. Bogorin, M. Brink, L. Capelluto, O. Günlük, T. Itoko, N. Kanazawa, A. Kandala, *et al.*, [Quantum Science and Technology **6**, 025020 \(2021\)](#).
- [30] Y. Guo, P. Taranto, B.-H. Liu, X.-M. Hu, Y.-F. Huang, C.-F. Li, and G.-C. Guo, [Physical Review Letters **126**, 230401 \(2021\)](#).
- [31] $\ell = 2$ and $\ell = 1$ models can be constructed from subsets of the $\ell = 3$ data, however on their own they minimally require $3 \times 300 = 900$ and $4 \times 30 = 120$ experiments per time, respectively.
- [32] R. Blume-Kohout, J. K. Gamble, E. Nielsen, K. Rudinger, J. Mizrahi, K. Fortier, and P. Maunz, [Nature Communications **8**, 14485 \(2017\)](#), [arXiv:1605.07674](#).
- [33] G. A. L. White, C. D. Hill, and L. C. L. Hollenberg, [Physical Review Applied **15**, 014023 \(2021\)](#), [arXiv:1911.12096](#).
- [34] D. Chruściński, A. Kossakowski, and A. Rivas, [Phys. Rev. A **83**, 052128 \(2011\)](#).
- [35] S. Pethel and D. Hahs, [Physica D: Nonlinear Phenomena **269**, 42 \(2014\)](#).